

ClimateSOM: A Visual Analysis Workflow for Climate Ensemble Datasets

Yuya Kawakami , Daniel Cayan , Dongyu Liu , and Kwan-Liu Ma 

Abstract—Ensemble datasets are ever more prevalent in various scientific domains. In climate science, ensemble datasets are used to capture variability in projections under plausible future conditions including greenhouse and aerosol emissions. Each ensemble model run produces projections that are fundamentally similar yet meaningfully distinct. Understanding this variability among ensemble model runs and analyzing its magnitude and patterns is a vital task for climate scientists. In this paper, we present ClimateSOM, a visual analysis workflow that leverages a self-organizing map (SOM) and Large Language Models (LLMs) to support interactive exploration and interpretation of climate ensemble datasets. The workflow abstracts climate ensemble model runs—spatiotemporal time series—into a distribution over a 2D space that captures the variability among the ensemble model runs using a SOM. LLMs are integrated to assist in sensemaking of this SOM-defined 2D space, the basis for the visual analysis tasks. In all, ClimateSOM enables users to explore the variability among ensemble model runs, identify patterns, compare and cluster the ensemble model runs. To demonstrate the utility of ClimateSOM, we apply the workflow to an ensemble dataset of precipitation projections over California and the Northwestern United States. Furthermore, we conduct a short evaluation of our LLM integration, and conduct an expert review of the visual workflow and the insights from the case studies with six domain experts to evaluate our approach and its utility.

Index Terms—Climate visual analytics, ensemble visualization, self-organizing maps

1 INTRODUCTION

Ensemble datasets are increasingly integral to scientific research as computing resources have increased in power [34, 66]. Many disciplines, from computational fluid dynamics [48] to material science [66], rely on ensemble datasets to capture and predict variability by running their models under different conditions and parameters. The result is a collection of model runs—an *ensemble dataset*—that supports exploration of possible outcomes, sensitivity analysis, and uncertainty quantification. However, working with ensemble datasets remains difficult due to their sheer size and complexity [66].

Climate science in particular relies on ensemble datasets to examine plausible climate futures under varying conditions, such as greenhouse gas and aerosol emissions or land use changes [17, 44, 47]. Each model run often represents a spatiotemporal time series, where each time step is a climate outcome (e.g., precipitation) over some spatial regions. These model runs may come from different global climate models [17, 44] and use varying input assumptions, producing a broad set of outcomes. Understanding and communicating the resulting variability and patterns remains a major challenge.

Although existing analyses in climate science provide valuable insights—often through statistical summaries like spatial means and variances across model runs—they may overlook key spatial and temporal structures [31]. Visual analytics techniques have been developed to support interpretation of ensemble data [8, 15, 31], but many struggle to provide both interpretability and robustness when dealing with highly complex, chaotic model behavior. In this context, even summarizing a single model run clearly is difficult, and comparing or clustering multiple runs poses a greater challenge.

To overcome these limitations, we introduce, ClimateSOM, a new visual analysis workflow that equips climate scientists with an intuitive tool and visual language for exploring and analyzing ensemble climate projection datasets. In line with findings by Wang et al. in their comprehensive survey of ensemble data visualization [66], we identify

three essential tasks when working with such datasets: (1) *exploring a single set of model run(s)*, (2) *comparing the behavior across two sets of model runs*, and (3) *clustering the behavior of multiple model runs*. These tasks are crucial for uncovering insights into climate variability and making meaningful inferences about these projections. These tasks along with its interpretability serves as our guiding principle.

The overarching goal for ClimateSOM is data abstraction by transforming spatiotemporal time series into a distribution over a user-steerable 2D space. Central to ClimateSOM is a self-organizing map (SOM) [35], a widely recognized analytical tool in climate science, along with steerable dimensionality reduction and annotations. Through this transformation, ClimateSOM enables flexible, interpretable exploration of diverse model behavior, helping researchers detect patterns and relationships that would otherwise be difficult to uncover.

We further integrate LLMs to assist in sensemaking of the SOM-defined 2D space. ClimateSOM introduces an LLM-empowered bidirectional query methods that allows users to (1) locate regions of interest in the 2D space based on natural language queries and (2) generate textual summaries of selected regions. We demonstrate the utility of ClimateSOM through case studies using LOCA-downscaled CMIP6 climate projections [49] across two regions in the western United States. In addition, we conduct an expert review with six domain scientists to assess the system’s usability and its ability to support scientific insight. In short, the contributions of this work are the following:

- A novel workflow for visual analysis of a spatiotemporal ensemble that abstracts the ensemble members as a distribution over a steerable 2D space framed by a self-organizing map.
- Integration of LLMs to assist in sensemaking of the SOM-defined 2D space in which ClimateSOM operates.
- ClimateSOM, a visualization interface that supports this workflow end-to-end, enabling users to explore, compare, and cluster ensemble model runs.

2 RELATED WORKS

2.1 Visual Analytics for Climate Ensemble Data

The increasing availability of ensemble data from large-scale climate simulations has led to the development of a range of visual analytics methods designed to manage and interpret uncertainty, spatial-temporal patterns, and inter-model variability [6, 8, 9, 18, 25, 31, 33, 67]. Past works have considered topology-based methods, where isocontours, spaghetti plots or similar methods are employed to encapsulate prominent spatial features while encoding ensemble variability [30, 32, 38, 43, 59].

- Yuya Kawakami, Dongyu Liu, and Kwan-Liu Ma are with University of California, Davis. E-mails: {ykawakami, dyuliu, klma}@ucdavis.edu
- Daniel Cayan is with Scripps Institution of Oceanography, University of California, San Diego. E-mail: dcayan@ucsd.edu

Manuscript received xx xxx. 201x; accepted xx xxx. 201x. Date of Publication xx xxx. 201x; date of current version xx xxx. 201x. For information on obtaining reprints of this article, please send e-mail to: reprints@ieee.org. Digital Object Identifier: xx.xxx/TVCG.201x.xxxxxx

Others have proposed graph-based representations of ensemble relationships [29, 62] or treated ensemble members as collections of images to facilitate comparative analysis [26]. Kappe et al. introduced a Sankey-diagram-based visualization using k -means clustering on the entire climate field to summarize variability in decadal predictions [31], while Evers et al. employed spatial correlation measures and multidimensional scaling (MDS) to embed ensemble members for comparative visualization [16].

However, in the context of visualizing the overall behavior of a single climate ensemble model run or its comparison, past works have mostly relied on summary statistics of the climate field interest or what Kappe refers to as the *mean field approach* [28]. Such approaches, as well as topology-based methods that often select most prominent spatial features to represent ensemble members for analysis and comparison [18], may crucially miss out of the different distributional nature of the ensemble members, both within one member and across members.

Departing from this *mean field* aggregation is a key motivation for ClimateSOM. Rather than reducing the ensemble to a single statistical summary or a topological feature, our approach models it as a 2D spatially organized distribution, preserving the variability with each model run. This allows us to capture fundamental differences within and across ensemble members that may be ignored under the *mean field approach*, while allowing us to succinctly formalize notions of comparison and clustering within the workflow. We use a SOM to maintain local topological relationships while revealing fine-grained differences between ensemble members. In contrast to prior systems, which typically support only isolated subtasks, such as single-run exploration or pairwise comparison, ClimateSOM provides integrated support for exploration, comparison, and clustering. This unified capability addresses a gap in existing climate ensemble visual analytics.

2.2 SOMs in Visual Analytics and Climate Science

Self-organizing maps (SOMs) [35] are commonly used for their ability to project high-dimensional data onto a structured, low-dimensional grid while preserving local topological relationships. This pseudo-continuous 2D layout enables spatial interpretation and supports visual pattern recognition. In visual analytics, SOMs have been used to structure time-series and spatial data, as demonstrated by Andrienko et al. in their analysis of crime patterns [5]. Beyond this, SOMs have been applied in diverse domains such as astrophysics and cytometry, where the preservation of local structure facilitates cluster identification and improves interpretability [11, 12, 14, 22, 53, 57, 63, 64].

In climate science, SOMs have often been used for pattern extraction, where extracted nodes represent particular spatial patterns that may be linked to known physical phenomena [42, 46, 55]. For more applications of SOMs in climate science or related areas, we refer the reader to [21, 23, 41, 61]. Regardless of the exact application, the trained SOM and its associated 2D node space must be interpretable by the user to be useful as this serves as the backbone for its use. Past works have mostly considered Sammon Mapping or Multidimensional Scaling (MDS) to understand the SOM-defined 2D space; however, these methods do not provide user control over the mapping process.

In ClimateSOM, we extend SOM-based approaches by integrating interactive visual analytics techniques. In particular, we augment the SOM node space with interpretability tools including user annotations, interactive dimensionality reduction, and LLM-empowered bidirectional queries. This allows domain scientists to both guide and interrogate the structure learnt by the SOM, moving beyond static representations and improving the transparency and utility of the latent 2D embedding.

2.3 LLMs for VIS

Natural Language Interfaces (NLI) [60] or LLMs have been increasingly applied to assist in visualization workflows [24, 69, 70]. Such systems show promise in helping users by generating interpretable annotations in visualizations or by providing a conversational interface to the visualization system [60, 68] which can aid in their sensemaking process [7, 54]. They have also been shown to alleviate the “cold-start problem” in information-seeking, helping users establish context and

find a starting point when navigating new information [40]. LLMs have also been successfully applied for Text-to-SQL tasks [36, 69] and for summarizing insights from and improve usability in visual analytics interfaces [70]. In fact, LLMs have been used in geospatial visual analytics systems as in [37] for gathering and summarizing insights in a geospatial context.

In ClimateSOM, we integrate LLMs more tightly into the system design by enabling bidirectional interaction between users and the SOM-defined latent space. This includes support for text-based queries into the embedding and automated summarization of regions in the latent space. This approach not only improves usability but also enhances the interpretive bandwidth of the SOM, particularly in settings where exploratory context is limited.

3 PROBLEM CHARACTERIZATION

We focus on ensemble datasets such as those produced by the Coupled Model Intercomparison Project (CMIP6) [17], which contain climate projections generated under a variety of input assumptions. Each simulation produces a spatiotemporal time series, referred to as a model run. The following terminology is used throughout:

- **GCM** (Global Climate Model): Mathematical models that simulate the Earth’s climate system, and are used to project future climate scenarios (e.g., MIROC6, ACCESS-CM2, etc.).
- **SSP** (Shared Socioeconomic Pathways) [56]: Pathways that examine how global society, demographics, and economics might change over the next century. In addition to the historical period, we consider three SSPs in this work: SSP245, SSP370, and SSP585, a low, medium high, and high greenhouse gas emissions future respectively.
- **Model run**: A unique climate projection and spatiotemporal time series, representing a member of the climate ensemble generated by a specific combination (GCM, SSP). The full ensemble consists of multiple such runs.

3.1 Design Goals

In the project, in consultation with a climate scientist (paper co-author) specializing in regional climate variability and changes, we identified three key questions that drive exploratory analysis of ensemble climate datasets, which informs our system’s design goals.

R1 “Q: What is the general behavior of the set A of model runs?”

A climate scientist wishes to understand the general behavior of a single model run or a set of model runs and its general tendencies as it relates to the climate projection it generates. For example, do the model run(s) consistently produce projection of a certain quality or does it vary over time?

→ **Requirement:** *Provide a visual language to explore the behavior of a single set of model runs over the entire temporal domain.*

R2 “Q: How does set A of model runs compare to set B of model runs?”

A climate scientist wishes to compare the behavior of two sets of model runs A and B to understand the differences in their projections. For example, does set A of model runs produce similar projections compared to set B of model runs? What overlapping qualities do they share and what climate projection qualities are unique to each?

→ **Requirement:** *Provide a visual language to compare the behavior of two sets of model runs over the entire temporal domain.*

R3 “Q: Which model runs or GCMs exhibit *similar* behavior?”

A climate scientist wishes to understand whether there are meaningful clusterings of ensemble runs and clustering of GCMs based on the SSP forcings. Do all ensemble runs produce similar results? Is the effect of SSP forcing similar on all GCMs?

→ **Requirement:** *Support clustering of ensemble model runs based and clustering of GCM based on their SSP forcings over the entire temporal domain.*

3.2 Abstracting the Model Runs Into a Distribution

Central to ClimateSOM is a self-organizing map (SOM) trained to capture the spatial variability of a climate ensemble dataset, while retaining its interpretability. An SOM is an unsupervised neural network

that projects high-dimensional data into a 2D grid while preserving the topological structure, making it useful for dimensionality reduction (DR). Training a SOM over a climate ensemble dataset yields a 2D SOM grid, with each SOM node representing a spatial pattern over the studied region. ClimateSOM leverages this capability to represent each model run within the ensemble as a distribution. Specifically, for each time step we first locate its best matching unit (BMU) in the SOM nodes, and allow the 2D position of that SOM node to represent that time step. Aggregating these positions across all time steps produces a 2D distribution defined by the set of BMU’s node locations. Fig. 1 presents the construction of the distributional representation.

Noteworthy in this construction, however, is the projection step of the initial 2D SOM grid. While the SOM nodes maintain local smoothness, they can have distortions globally [61]; thus, defining the SOM node locations solely by their 2D grid location is not desirable. To address this, we add a projection step of the SOM nodes to better preserve their relative structure and enhance its interpretability.

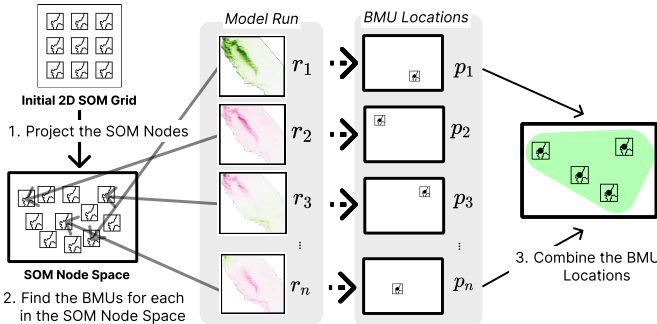


Fig. 1: The distributional abstraction for model runs in ClimateSOM. Each model runs are abstracted to a distribution defined by a projected location of SOM Nodes, the *SOM Node Space*.

Formally, for an ensemble run with n time steps, each of which a climate projection over some spatial domain, $R = [r_1, r_2, \dots, r_n]$, we abstract this as a set of points in 2D space:

$$S = \{p_1, p_2, \dots, p_n\}, p_i = \text{proj}(BMU(r_i))$$

where $BMU(r_i)$ is the best matching SOM node for r_i , and $\text{proj}(\cdot)$ maps the node to a 2D layout. This distributional representation of the model runs serves as the backbone of ClimateSOM.

3.3 Workflow Overview

The workflow contains one pre-step and three main steps (Fig. 2).

S0 Training the SOM The workflow begins with training the SOM on the dataset to ensure it has sufficient explanatory power—specifically, that the approximation via its BMU is adequate—and smoothness across the SOM grid.

S1 Anchor Using the pseudo-2D smooth SOM nodes from Step 0, this step enables users to create the *Adjusted SOM Node Space* by projecting the SOM nodes into a 2D layout. To support interpretation and navigation, users can anchor specific nodes—fixing their positions while allowing others to adjust—resulting in a more interpretable spatial arrangement than the original SOM grid. We refer to this refined space as the *Adjusted SOM Node Space*.

S2 Annotate Once the *Adjusted SOM Node Space* is defined, users annotate it to produce the *Annotated SOM Node Space*. An annotation consists of (1) a bounded region within the adjusted space and (2) a text label describing that region. These annotations serve as an abstraction layer to facilitate interpretation in the next step. ClimateSOM incorporates LLMs to assist with this process.

S3 Analyze A given model run can now be described as a distribution within the *Annotated SOM Node Space*. This distribution can be further broken down by user-defined *annotations* by considering the number of time steps of that fall within each *annotation* region **R1**. Model runs can be compared either by directly comparing their

distributions or by interpreting them as vector fields over the annotated space **R2**. Clustering can be applied to model runs based on these distributions, and to SSP forcings over each GCM by clustering changes in their respective distributions **R3**. Details are in Sec. 4.

Having outlined the workflow, we now address two important design choices: the use of SOMs and the intentional abstraction away from temporal ordering.

SOM as the central tool. We choose SOMs over other DR or clustering methods for the following two reasons:

- Preservation of local topology:** SOMs preserve neighborhood relationships in lower-dimensions which enables meaningful spatial interpretations. Our distributional abstraction of model runs requires that the learned grid be continuous and neighboring nodes express similar spatial patterns. Other DR or clustering methods do not produce topologically smooth results in lower-dimensions and thus do not satisfy the conditions required in ClimateSOM.
- Established use in climate science:** SOMs are widely used for analysis of climate data and are familiar to domain experts, aiding in its interpretation.

Ignoring the temporal ordering. ClimateSOM represents a model run R as a set of points S , thus discarding temporal order (scrambling R yields the same S). This is an intentional trade-off for two reasons:

- Emphasis of broad patterns:** The goal is to analyze the general behavior of model runs over time rather than their specific sequence. This aligns with how GCM outputs are studied for broad differences in climate science.
- Reducing complexity:** While preserving temporal order enables the use of time series analysis techniques, such as dynamic time warping, it also introduces complexity and amplifies the random variations inherent in climate ensemble data.

This trade-off enables simpler interpretation while retaining the ability to extract broad patterns from model outputs.

4 CLIMATESOM

4.1 Training the SOM (S0)

For our spatiotemporal ensemble dataset, we train the SOM on the flattened ensemble dataset (i.e. across all spatial realizations that occur in the ensemble). As common choice, we opt for the neighborhood function $h(t)$ to be the Gaussian function and linearly decrease its σ as is standard practice in climate applications [21]. After training, the grid of SOM nodes is expected to approximate and learn the distribution input ensemble dataset under the constraint that the 2D grid of nodes are pseudo-smooth.

The SOM must meet two competing criteria: (1) it should retain sufficient information from the input data, and (2) the 2D grid of nodes should be smooth enough to avoid disconnections after projection, which would hinder interpretability. However, these two criteria are often in conflict. A smaller neighborhood update size captures finer details of the data’s topology but results in a less smooth SOM grid, as each update affects a smaller region. Conversely, a larger update size smooths the grid but may obscure finer details. We found that the choice of (1) the initial neighborhood update size ratio expressed as a ratio between the initial update size and the dimension of the SOM grid, ($kR = (\sigma_{initial})^2 / dim^2$), and (2) the ratio of the final neighborhood update size, $kS = \sigma_{final} / \sigma_{initial}$, to the initial size at the first iteration (kS) are critical to balancing these two criteria. For our case studies, we found that $kR = 0.03$ and $kS = 0.2$ provide balanced results. Further details are in the Appendix.

4.2 Anchor (S1)

As seen in past works in climate science employing SOMs [61], the SOM grid, while constructed to be locally smooth due to the training process, can have distortions globally. Therefore, SOMs are often presented alongside Sammon maps [58] or Multidimensional Scaling (MDS) to provide a more faithful view of the SOM grid in terms of its relative distances between nodes. However, these methods give users no control of the mapping process and gives priority to global structure

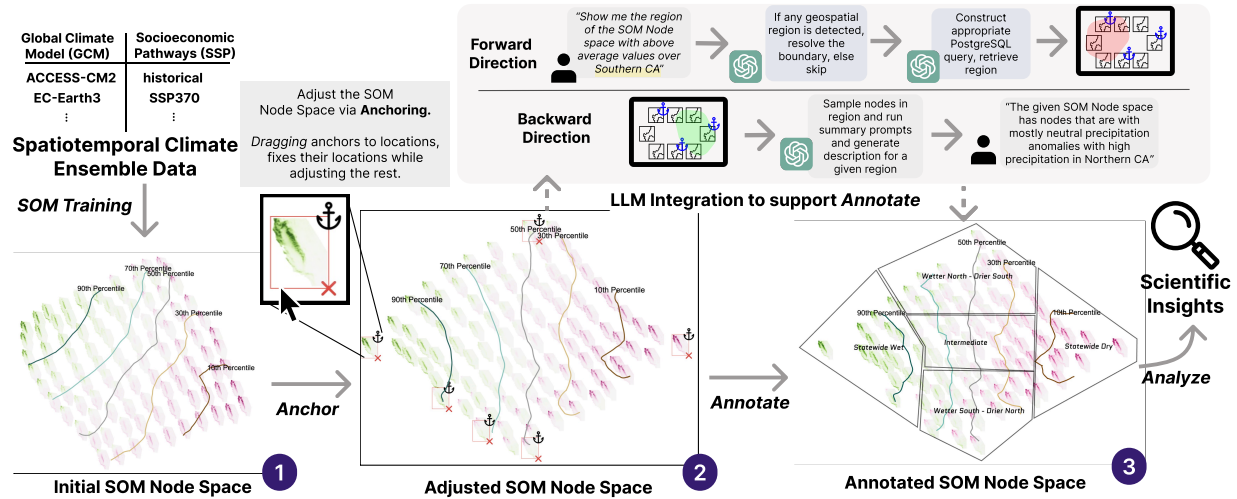


Fig. 2: The ClimateSOM workflow. The workflow is composed of the SOM Training step and three main steps: Anchor, Annotate, and Analyze. In **S1**: Anchor, the user adjusts the Initial SOM Node Space ① using iterative anchoring with Minimum-Distortion Embedding to produce the *Adjusted SOM Node Space* ②. Dragged nodes are called *anchors* and are fixed in place, while the rest of the nodes are adjusted. In **S2**: Annotate, the user annotates the SOM Node Space using manual inspection of the SOM Nodes or with the LLM Integration. Once annotated, in **S3** the user can use the *Annotated SOM Node Space* ③ as the basis to analyze the ensemble dataset.

in place of local structure. To provide users with the iterative ability to shape and project the SOM nodes, we allow user to *anchors* particular SOM node in the projection process. The utility of placing constraints on DR processes has been explored in previous works [65], and we find the iterative nature of anchoring to be most suitable as it requires minimal intervention from the user.

In ClimateSOM, we employ Minimum-Distortion Embedding (MDE) [4] to support anchoring. Similar to UMAP [45], MDE can be presented as an optimization problem over local neighborhood graphs. Using MDE, we optimize for the distortion of the SOM grid nodes in the 2D space while anchoring points in the output space to ensure a more meaningful layout of the SOM nodes. In our UI, dragging the SOM Nodes designates them as *anchored* and are fixed in place in the projection, while other nodes are adjusted. This anchor step allows users to (1) physically map the two main axes of variation that the 2D SOM extracts to the visual interface and (2) semantically map nodes to appropriate locations in the screen. (e.g. SOM nodes with high value in the *north* be placed in the *upper-half* of the screen.) We find that fine adjustments like encouraging specific nodes to be positioned at particular locations required iterative methods. This anchoring interaction was well suited, and thus included in ClimateSOM. We refer to the output of this step as the *Adjusted SOM Node Space*.

4.3 Annotate (S2)

This step allows users to provide *annotations* to the *Adjusted SOM Node Space* to add user-defined context to the SOM nodes in preparation for subsequent analysis in **S3**. We define an *annotation* as a pair of the following: (1) a bounded region within the *Adjusted SOM Node Space* and (2) a text label that describes the region. Two challenges arise: identifying relevant regions and defining meaningful labels. Given the documented success of Text-to-SQL via LLMs [69] and text summarization [52], our approach for ClimateSOM is leveraging LLMs in this process, alongside the user’s visual inspection of the individual SOM nodes. These correspond to the forward and backward directions of LLM assistance as shown in Fig. 2.

4.3.1 Forward Direction

In the forward direction, we assume the user has a characteristic of interest in mind for SOM nodes (e.g., “Show me SOM nodes with average precipitation over Southern California above 0”). The goal is to identify the corresponding region in the *Adjusted SOM Node Space* by filtering nodes that match the specified condition. This is done by generating a PostGIS query based on the user’s geospatial query. However, we found that naively prompting this task to the LLM does not yield consistent results, primarily due to LLM’s lack of accuracy in

generating appropriate boundaries for given geospatial regions as found in [39]. To address this, we delegate the LLM not to generate spatial boundaries, but instead to generate a list of counties that correspond to the named region. These counties, which have well-defined boundaries, are then used to construct the spatial filter, reducing errors introduced by the LLM. In all, the forward direction proceeds as follows.

1. Parse the user query to detect any region names or locations. If none are detected, skip to step 3.
2. Resolve the identified regions to a list of counties with known boundary definitions. Combine these county boundaries to form the target region.
3. Use the resolved region and the numerical conditions extracted from the query to construct and execute a PostGIS query over the SOM nodes.

Supported Question Types Based on discussions with the domain experts, we identify three categories of user queries that the LLM should be able to support by generating appropriate PostGIS queries:

1. SOM nodes such that the average value over *some geospatial region* is above / below X
2. SOM nodes such that the average value over *some geospatial region* is between X and Y
3. SOM nodes such that the average value over *some geospatial region A* is higher or lower than the average value over *some geospatial region B*

4.3.2 Backward Direction

In the backward direction, we presume the user has identified a region within the *Adjusted SOM Node Space* and wishes to get a high-level summary of the region. In ClimateSOM we accomplish this as follows.

1. Given a region in the *Adjusted SOM Node Space*, we extract samples evenly within the SOM Node Space region.
2. Construct a per-county level summary statistics of each node from step 1. For a given sampled SOM node, we textually represent as:

```
{ high:[counties_list], mod_high:[counties_list],
  neutral:[counties_list], mod_low:[counties_list],
  low:[counties_list] }
```

That is, we enumerate all counties with average values in each of the five categories. Note that, we allow the cutoff values that define *high*, *moderately high*, etc. to be modified by the user.

3. Use the text-based summary statistics for each sampled SOM node with the LLM to generate a summary description of the region.

In summary, the LLM is used in the forward direction for two tasks: (1) mapping region names to a list of counties, and (2) generating PostGIS queries to retrieve relevant SOM nodes. In the backward direction, the

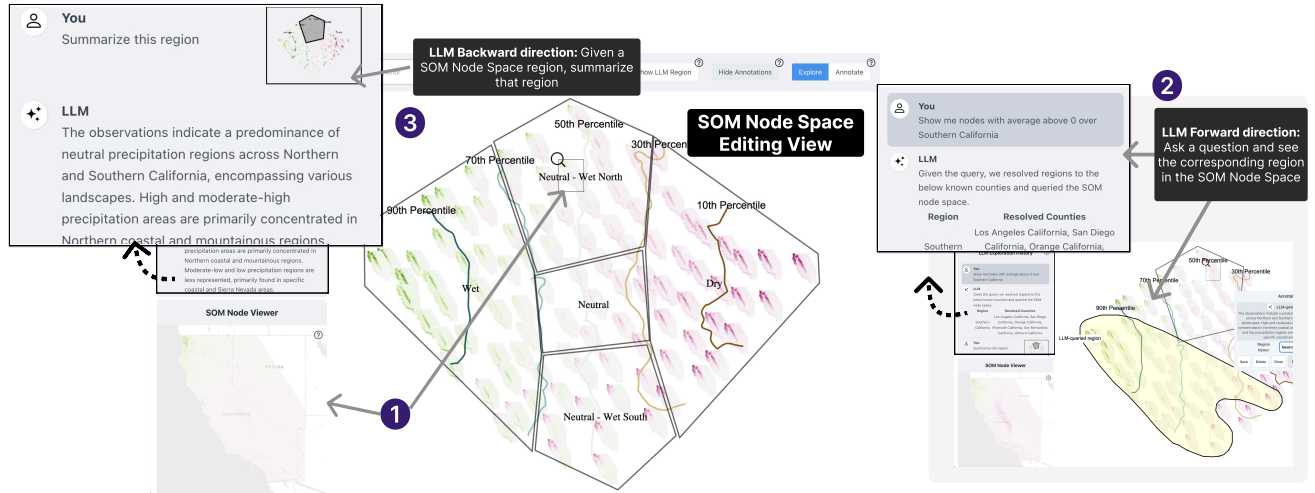


Fig. 3: The ClimateSOM interface at the end of **S1** and **S2** displaying the *Annotated SOM Node Space*. The user can inspect each SOM node via clicking on the node **1**, and the Node Viewer on the left displays the selected map of the SOM Node. To support **S2**: Annotate, users can leverage the two directions of LLM-powered query system: Forward **2** and Backward **3**. For the forward direction **2**, the user can request a particular quality of interest, (e.g., *Show me nodes that have average above 0 over Southern California*) and be presented with the corresponding SOM Node region bounded in yellow. For the backward direction **3**, the user can right click on a SOM Node region and a LLM will generate a ~50-word summary of SOM Node realizations in that region. Through visual inspection and the LLM assistance, the user compiles the set of *annotations* as regions in the SOM Node Space and a label corresponding to the region.

LLM serves as a summarizer of per-county statistics derived from user-selected regions. We implement both directions using LangChain [2] with OpenAI’s *gpt-4o-mini* [3] and use LangChain Tools for the forward direction to detect if the user input includes any geospatial regions that need to be resolved. Details of the prompts used are available in the Appendix. Either via manual inspection of the *Adjusted SOM Node Space* or via the LLM integration, the user can now define a set of *annotations* for the *Adjusted SOM Node Space* to produce the *Annotated SOM Node Space*.

4.4 Analyze (S3)

Finally in this step, we describe how ClimateSOM performs each of the tasks and meets the design requirements outlined in Sec. 3.1.

4.4.1 Exploring a single set of model runs R1

Given a single ensemble model run with n time steps, $R = [r_1, r_2, \dots, r_n]$, we can describe it as a distribution $S = \{p_1, p_2, \dots, p_n\}$ within the *Annotated SOM Node Space* by mapping each r_i to its best BMU and applying the MDE projection: $p_i = MDE(BMU(r_i))$. We then compute a kernel density estimate (KDE) over S , which serves as a “fingerprint” of the model run. Regions of high density indicate spatial patterns that occur frequently in the run (Fig. 6-1). This distribution can also be expressed as percentages over the annotated regions defined in **S2**, enabling semantic interpretation beyond the KDE plot (Fig. 6-2). For a set of multiple model runs, we apply the same process over the entire set and consider the set of all points as the representative distribution.

4.4.2 Comparing the behavior of two sets of model runs R2

To facilitate comparison of two model runs R_1 and R_2 , ClimateSOM provides two methods: (1) side-by-side comparison and (2) a vector field formulation.

Comparison via side-by-side The side-by-side comparison is a direct comparison of the distributions of R_1 and R_2 in the *Annotated SOM Node Space* as defined in Sec. 4.4.1. By presenting these two views side-by-side, we allow users to visually inspect if there are regions within the SOM Node Space that are occupied in similar densities or different densities by R_1 and R_2 (Fig. 5). Similar to the exploration of a single model run, the respective distributions can be compared via the breakdown based on the annotations defined in **S2** Annotate.

Comparison via a vector field formulation We also support a formal comparison using vector fields, based on a bootstrap approach [13] (implementation details in the Appendix). Given two model runs R_1 and R_2 , we generate k number of bootstrap samples for each model run. At each iteration, we first calculate the 2D optimal transport [19]

between the two bootstrap samples. Given the optimal transport plan, we construct a set of vectors for each pair in the transport plan that points from its source to its target. Interpolating the results for the set of vectors onto a regular grid generates a vector field, representing the spatial transition from R_1 to R_2 (Fig. 6-3). The resulting field represents the spatial transition from R_1 to R_2 . This further enables analysis at the level of annotations—e.g., determining where points from annotation A in R_1 are mapped in R_2 (Fig. 4).

This approach is particularly useful when comparing temporally ordered scenarios (e.g. comparing a historical run to a future run or comparing a low to a high emission scenario). The vector field comparison may provide an added layer of context since the comparison is treated as a *transition* from one to the other. When comparing between two sets of model runs, we apply the same process to the aggregated set of points in each set as was in **R1**.

4.4.3 Clustering the behavior of many model runs R3

Clustering model runs directly Given the distributions of the model runs in the *Annotated SOM Node Space*, we perform clustering using Earth Mover’s Distance (EMD) [19] to quantify the similarity producing a distance matrix between the distributions. We then apply UMAP on the distance matrix to produce a 2D embedding and HDBSCAN [10] to perform the clustering. While HDBSCAN can operate on the distance matrix directly, we found more consistent results using this two-step method. This results in a clustering of model runs that exhibit *similar* and *dissimilar* behavior, where each cluster can be represented as an aggregate distribution of the model runs in that cluster.

Clustering GCMs based on their SSP forcing Given vector field formulation of forcing (i.e., the effect of an emission future as a *transition* from the historical time period), we perform clustering of the vector field using an average cosine similarity to quantify the similarity between the vector fields. Similarly, we can use UMAP and HDBSCAN to perform clustering such that we can identify GCMs that exhibit *similar* and *dissimilar* behavior under the same SSP forcing. For this variant, each cluster can be represented as a vector field that represents the average forcing of the GCMs in that cluster.

A notable design implication of ClimateSOM and its formulation is that the resulting clustering is interpretable, since it can be displayed directly in the same *Annotated SOM Node Space* as distributions or vector fields. We consider this explainable clustering results as a key strength of ClimateSOM (Fig. 6-4).

5 THE VISUAL INTERFACE

To introduce the interface design for ClimateSOM, let’s consider a climate scientist with a climate ensemble dataset of monthly precipitation projections over California, expressed as anomalies from historical averages. Given this ensemble, we assume the scientist is interested in the three research questions introduced in Sec. 3.

Assuming **S0** is complete, the trained SOM is a 2D grid of SOM nodes, where each node is a precipitation map over California. Then the scientist proceeds through **S1** and **S2**.

5.1 SOM Node Space Editing View

The main visual component for ClimateSOM is the trained SOM and the SOM Node Space that the user iteratively edits as seen in Fig. 2. The SOM Node Space Editing View supports the anchoring and annotating of the SOM Nodes in **S1** and **S2**. For our case studies, displaying all SOM Nodes risks unnecessary clutter. As such a subset, 100 in the case studies, are rendered. This was determined via trial and error, optimizing for minimal occlusion whilst maintaining enough nodes to communicate the node structure. First, as in Fig. 2-1, the *Initial SOM Node Space* is presented to the user using the unanchored MDE result, with each node depicting a precipitation map over California using a Green-Pink (high-low precipitation) colormap. The interface also presents colored percentile lines in the SOM Node Space to orient the user to the mean anomaly in each SOM node.

In **S1** the user constructs the *Adjusted SOM Node Space* by anchoring and reflecting the anchors via MDE. SOM nodes in this step can be dragged around freely, and nodes that are set to be anchored are displayed with an anchor icon as seen in Fig. 2. Furthermore, they can be inspected further by clicking on the node, displaying that node in the SOM Node Viewer (Fig. 3-1). Once they have a satisfactory *Adjusted SOM Node Space* they proceed to **S2**. Right clicking within the *Adjusted SOM Node Space*, users can define vertices for each *annotation* polygon. This step constructs the *Annotated SOM Node Space* by leveraging the LLM-empowered bidirectional query system in addition to manual visual inspection. The interface supports two directions of LLM integration, forward (Fig. 3-2) and backward (Fig. 3-3), to assist the user in defining annotations. The interface provides the history of the user’s interaction with the LLM in a chat-like visual UI. Annotations as seen in Fig. 3 are rendered as bounded regions in the *Annotated SOM Node Space* with a user-defined label. This label can be produced via the user’s inspection of the bounded region in question, or with assistance from the LLM’s ~50-word summary of the region. Once all annotations are defined and named, the *Annotated SOM Node Space* is ready for analysis in **S3**. Fig. 6 provides an overview of the visual interface support for **S3**.

5.2 Model Run Inspection and Characteristic View

First in pursuit of **R1**, the user can inspect a single model run over any given month by selecting them via a dropdown menu and view its distribution over the *Annotated SOM Node Space* in the Model Run Inspection View (Fig. 6-1). The interface presents the 2D distributional representation of the selected model run as a KDE plot drawing three polygons as of the top 25%, 50%, and 75% density regions. Thus, the darkest areas of the KDE plot correspond to the SOM Node Space regions with the highest density of realizations in the selected model run. In addition, we provide the breakdown of that model run’s behavior broken down by the annotations in the Characteristic View (Fig. 4). In the Characteristic View, the distribution for the selected model run is broken down by the annotations, presented alongside a node map glyph (Fig. 4-left), ordered by its percentages in each annotation region. The node map glyph is designed to quickly direct the user to the SOM Node Space region that each annotation represents. Furthermore, in the case that the user is comparing two model runs as a vector field, the Characteristics View instead displays the *transition* as a Sankey diagram between the annotations.

Justification: In exploring the behavior of model runs, the primary goal for climate scientists is to understand where the hotspots are. That is, which part of the SOM Node Space most of the realizations of the model runs are concentrated. To this end, we employ the KDE



Fig. 4: The Characteristic Viewer for inspecting single model run and when comparing two model runs as a vector field.

representation as the visual encoding for the distribution so that we draw the most attention to the hotspots in the distribution. Other designs we considered include using a 3D representation and encoding the density in the height, but we found a 3D encoding less effective as it was more difficult to interpret. The Characteristic View is designed in a similar vein, to provide a quick overview of the distribution of the model run over the annotations provided in **S2**, and the node map glyph directing the user to the hotspots at the level of annotations in the distribution.

5.3 Model Comparison View

To support **R2**, we offer two visual interfaces for comparing two model runs: via a side-by-side comparison and as a vector field. First, the side-by-side comparison allows for simple visual comparison of two model runs, by placing the two distributions side-by-side in the *Annotated SOM Node Space* (Fig. 5). By drawing the distributions over the identical SOM Node Space, the user can quickly identify the SOM Node Space regions where the densities differ. However, to support the user for comparative tasks where there is a natural order to the comparison (e.g., comparing the same GCM over the historical vs. future period), we provide a vector field comparison view as well (Fig. 6-3).

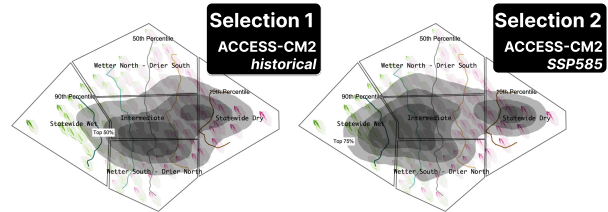


Fig. 5: The side-by-side comparison view for comparing two model runs.

Justification: Although the side-by-side comparison is simple to interpret, there were cases where the differences were subtle, or when we could infer an ordering, there was scope to provide a simpler visual encoding for the comparison. We found that the vector field representation was a good fit for this task as the direction of the arrows provided a natural interpretation of the comparison as a *transition*.

For the vector field formulation of the comparison, we initially used a particle advection animation similar to those used in flow visualization but found that the static vector field representation to be more simple and required less visual processing. In all, the two methods for comparison were well received by our domain expert, and thus implemented in the final design.

5.4 Clustering View

Lastly, to support **R3**, clustering results (Sec. 4.4.3) are visualized as a circuit-line diagram connecting the independent per-month clustering results (Fig. 6-4). For our scientists, in addition to understanding the results of the per-month clustering results, there is also interest in understanding the evolution of the monthly clustering results. That is, how the cluster membership of a model run changes over different months.

Each monthly cluster is represented as a box and the model runs are visualized as lines through the boxes, indicating its cluster membership for the given month. The cluster boxes are colored according to the cluster’s mean anomaly, and the lines according to the model run’s SSP. We compute a 1D MDS with intercluster distances as the distance matrix for each month, and the cluster boxes are placed according to this result. Therefore, for every month, more similar clusters are placed closer together and less similar clusters further apart. In the clustering

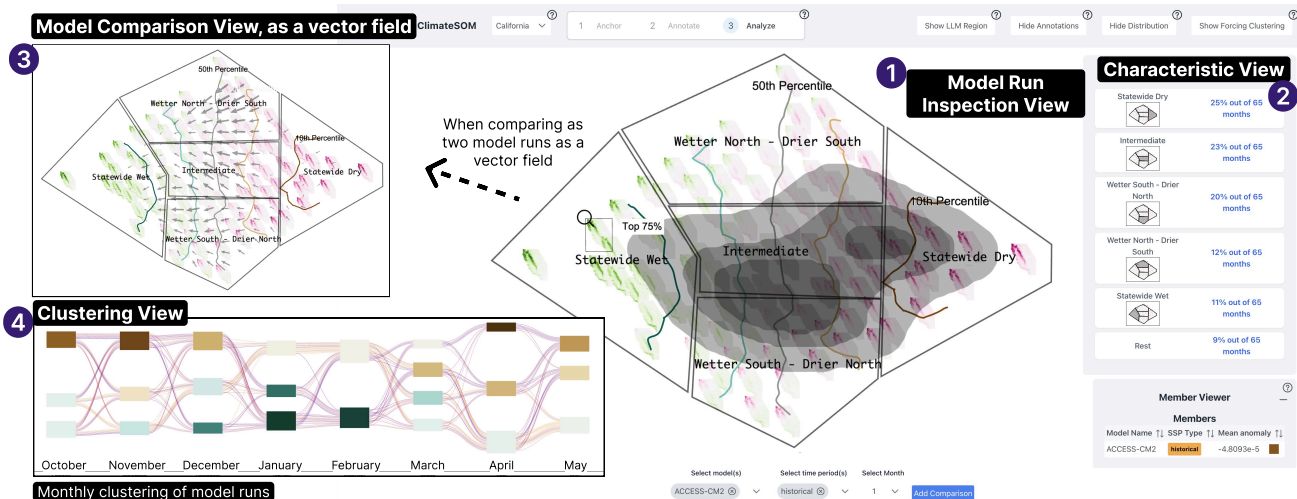


Fig. 6: The visual interface to support the last step — **S3** Analyze. Each selected model run is displayed as a distribution over the *Annotated SOM Node Space* **1** and the breakdown of the distribution over the annotations are displayed in the *Characteristic View* **2**. To support comparison, this main interface also supports a side-by-side comparison (Fig. 5) but also as a vector field **3**. Lastly, to support clustering of model runs or GCMs by SSP forcing, the circuit-line diagram displays the monthly clustering results and their evolution **4**.

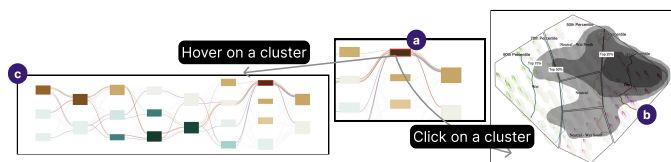


Fig. 7: Clicking **a** on a monthly cluster model run clustering variant Fig. 6—**4** will select model runs represented in that cluster **b** and show its distribution over the *Annotated SOM Node Space*. On hover, only lines that pass through the hovered cluster are highlighted **c**.

diagrams, tracing each line provides a sense of the evolution of the clustering results over the months. To support the investigation of the behavior of each cluster, clicking on a cluster will trigger the display of the data of that cluster as seen in Fig. 7. Furthermore, to support the user in understanding if there are inter-month relationships between the clusters, we implement a hover interaction as well, by allowing the user to filter the lines based on those that pass through that hovered cluster. A similar visual encoding supports the second variant of clustering—GCMs by forcing. For this variant, each line represents GCMs instead of model runs as the GCMs are the subject of clustering.

Justification: As seen in works like [27] where the patterns in the data and the evolution of patterns are the subject of inquiry, we apply a similar approach utilizing 1D MDS, letting the x-axis represent time and y-axis represent similarity. Supporting the analysis of inter-month relationships in addition to the per-month clustering results was a key interest expressed by our domain expert, and thus we choose this design.

6 EVALUATION

6.1 Case Studies

The Data To demonstrate that ClimateSOM can uncover valuable insights, we apply the workflow to an ensemble dataset of LOCA-downscaled CMIP6 precipitation projections [17,50,51] over California and the Northwest United States [49]. These model projections were made under 3 different SSPs [56], from a SSP245, a relatively low greenhouse gas emission future, SSP370, a medium high greenhouse gas emissions future, and SSP585 a high greenhouse gas emissions future. We consider 14 GCMs for each SSP and the historical period (i.e. four time periods per GCM) for which data was available, resulting in a total of 56 ensemble members. Details of the ensemble members used in this work can be found in the Appendix.

We consider two regions separately: California and the Northwestern United States, encompassing Oregon, Washington, and Idaho. While daily predictions are available, we focus on monthly projections considering months from October to May, as these months contribute to ~85% of the annual precipitation in both spatial regions. In addition,

we normalize the monthly anomalies by dividing them by per-month standard deviation across models, time, and space. The final data, therefore, consists of monthly precipitation anomalies expressed in standard deviations from the historical average. SOMs were trained on this monthly anomaly data across *all* months, SSPs, and GCMs to best capture the overall anomaly structure. For the California case study, each ensemble model run had a size of $65 \times 12 \times 151 \times 165$ (years \times months \times longitude \times latitude), while for the Northwestern US, it was $65 \times 12 \times 60 \times 115$. We consult **E1**, a climate scientist and a co-author of this paper, for the California case study, and another domain expert **E2** for the Northwestern US case study.

6.1.1 LOCA-Downscaled CMIP6 over California

SOM Training We experimented with various dimensions of the SOM grid and found that the choice had minimal impact on the results so long they were sufficiently large and selected a 30×30 grid. We include the impacts of the initial neighborhood radius ratio kR and the neighborhood decay ratio kS on the SOM in the Appendix. For the California region, we selected $kR = 0.03$ and $kS = 0.2$ as they provided a good balance explanatory power and SOM grid smoothness. This provided a SOM grid with 80.5% of explained variance.

The Case Study We outline a case study of the precipitation ensemble over California with the **E1**, a climate scientist and co-author of this paper. We will reference Fig. 8 for this case study. First, the expert goes through **S1**: Anchor to reorganize the SOM node space to improve the interpretability of the SOM node space. They place wetter precipitation SOM nodes to the left, dryer nodes to the right, and allow the vertical axis to represent the North-South gradient of the region, placing nodes with higher precipitation in the North on the upper side of the SOM Node Space and vice versa. The LLM-integration reported the area within the *Adjusted SOM Node Space* with negative and positive precipitation over the counties over Southern and Northern California, indicating a presence of SOM nodes with positive precipitation in Southern California and negative precipitation overall. Next, along with manual inspection of the space, they perform **S2**: Annotate producing five annotations regions: (1) *Statewide Wet*, (2) *Wetter North - Drier South*, (3) *Wetter South - Drier North*, (4) *Intermediate*, and (5) *Statewide Dry* (Fig. 2—**3**). The first question the expert wishes to answer is on the behavior of model runs that predict a wetter California in January and whether there are trends that these model run exhibit in the previous months. To this end, the expert examines the model run clustering in the circuit-line diagram and identifies two clusters of model runs in January (**R3**), one representing a wetter California than the other based on the color of the cluster boxes.

They then compare the two January clusters (**R2**), learning that

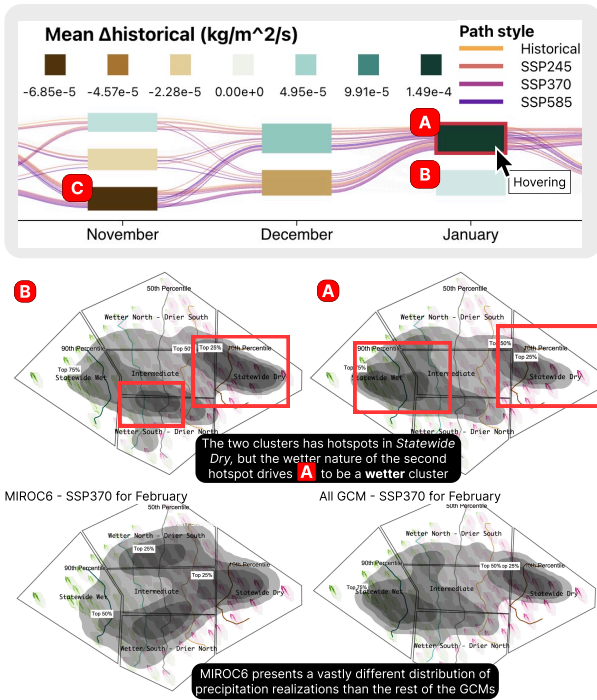


Fig. 8: The California case study. The Annotated SOM Node Space used is shown in Fig. 3. The expert explored monthly clustering in model runs in January - here the user has hovered over **A**, displaying the lines that pass through it (**R3**). The expert explored the cluster behavior by examining its distributions. Lastly, they also explored a single model run, *MIROC6 - SSP370*, against the same SSP for all GCMs (**R2**).

the difference in the two clusters (**A, B**) is primarily in the density of *Statewide Wet* realizations. Interestingly, the *Statewide Dry* realizations are both prominently present in both clusters. They visually confirm that the additional occurrences of *Statewide Wet* realizations in one cluster is the driving difference between the two clusters. Further, they learn from the circuit-line diagram that the both the drier and wetter cluster in December evolve to a wetter California in January, but realizes that it primarily evolves from a dry cluster in November considering the number of lines that pass through the respective clusters. Following the dry cluster in November [**C**], they learn that this cluster is represented by heavy *Statewide Dry* realizations as well as *Wetter South - Drier North* realizations. Thus the expert concludes that models run that predict a wetter California in January are associated with an overall drier November with a particular dryness in the North of the region, but less clear trends in December.

Another exploration that the expert wishes to undertake is of the behavior of *MIROC6*, a GCM, in the medium-emission scenario, *SSP370*, relative to the other GCMs under the same emissions scenario. Exploring through different months, they observe that *MIROC6* in February has a distinct pattern compared to the other GCMs in the same emissions scenario. While the other GCMs over February are distributed across *Statewide Wet* and *Statewide Dry* realizations, *MIROC6* introduces heavy *Wetter North - Drier South* and *Wetter South - Drier North* realizations (**R1**). This difference in mixture of realizations may warrant further investigation into *MIROC6 - SSP370* over February to understand the reasons for the model run's distinct behavior.

6.1.2 LOCA-Downscaled CMIP6 over the Northwestern US

We follow the same process to pick the SOM parameters for the Northwestern US case study, selecting $kR = 0.03$ and $kS = 0.2$ over a 30×30 SOM grid explaining 78.8% of the variance. With consultation from an Economist, **E2**, with experience studying in climate change impacts on the Western Coast of the United States, this case study examines LOCA-downscaled CMIP6 precipitation ensemble over the Northwestern US. We will refer to Fig. 9 for this case study. First, the expert goes through **S1**: Anchor to reorganize the SOM node space to improve the

interpretability of the SOM node space and **S2**: Annotate and visually identifies regions of interest, relying on previous domain knowledge of precipitation patterns in the Northwestern US. This yielded five annotated regions: (1) *Dry Global*, (2) *Wet NE*, (3) *Dry SW*, (4) *Wet Global*, and (5) *Remainder*.

First, the expert wishes to compare historical and *SSP585* precipitation projections in April. Here, this transition is represented by a change from a unimodal distribution of precipitation realizations to a bimodal distribution (**A**). In particular, the expert notices a shift to a wetter Northeast (of the region) under this higher emissions future, which they recognize to be a *notable change* with particular significance to agriculture in the region (**R2**). In contrast, in November, the expert observes a movement towards a wetter Northwest (of the region) in a higher emissions future. The expert therefore confirms that the effect on a higher emissions future on precipitation in the Northwestern US is drastically **different** between April and November, where April expects higher precipitation in the Northeast compared to the Northwest. This is an interesting insight, as simple statistical analysis would not reveal such spatial patterns.

Next, the expert wishes to explore whether there are outlier GCMs that exhibit different SSP forcing from historical to *SSP585* in November. Consulting the circuit-line diagram for the GCM clustering of forcings, they observe two clusters of GCMs in November, so they click on the two clusters, inspecting their forcing difference via the vector-field formulation. Here, they observe that one of the clusters (**B**), "*homes in the lower right area of the SOM distribution*" thus representing GCMs that predict a drier November with drier anomalies concentrated toward the Southwest of the region. On the other hand, the other cluster of GCMs (**C**), in contrast, collects toward the lower left area of the SOM distribution, and thus a wetter coastal region and wetter border with Canada, highlighting the two clusters of GCMs in its SSP forcing (**R3**). They hypothesize that the GCM's forcing in the first cluster may be anomalous, and thus may warrant further investigation. Throughout this session, the expert was impressed with *ClimateSOM*'s ability to "*visualize big picture patterns quickly*" and that it was "*just not something (they) could do otherwise*".

6.2 Evaluating the LLM integration

While past works demonstrate the ability of LLMs to generate SQL queries and a general text summarizer, past works on LLMs have not explicitly evaluated two spatial abilities: (1) the spatial ability to map region identifiers to a list of counties and (2) the spatial ability to summarize a list of counties to a short summary. Additionally, given the possible ambiguity that may arise in how places are defined (i.e., *Southern California* may mean different boundaries to different people), we conducted a short evaluation of our LLM in the above two tasks with 8 participants all familiar with the geography of California.

First, given a common region identifier (e.g., *Southern California*), we asked the participants to evaluate how reasonable the list of counties generated by the LLM was. Second, given a list of counties randomly selected from one of the textual summaries of a SOM node in the California case study, we asked the participants to evaluate how reasonable the regional summaries were. Both tasks were evaluated on a 5-point Likert scale. (1: *Strongly Agree*, 2: *Agree*, 3: *Neither Agree nor Disagree*, 4: *Disagree*, 5: *Strongly Disagree*). We show examples of the tasks in the Appendix.

Collecting 10 responses of each tasks (80 responses per task), we found that for T1, the average score was 2.11 (SD=1.32) and for T2, the average score was 2.5 (SD=1.55). This suggests that while our LLM was not perfect, they are able to generate reasonable lists of counties and summaries of regions that most participants found reasonable. Admittedly, in the first task there were regions where responses were more polarized, especially for vaguely defined region identifiers like *Desert Region of California*; and in the second task, when the list of counties were highly disconnected geographically, generating textual summaries of such regions was more challenging. Another limitation of the current implementation is that we use counties as the unit of analysis. However, natural language descriptions of regions do not always

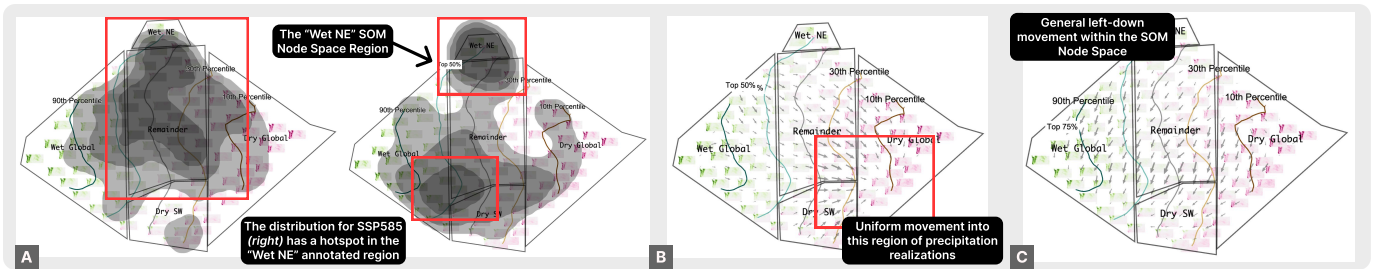


Fig. 9: The Northwestern US case study with ClimateSOM. **A**: Comparing historical and SSP585 projections in April (**R2**), **B**, **C**: Exploring the two GCM forcing clusters in November and comparing their behavior (**R3**).

conform to county boundaries—some regional identifiers may span or divide multiple counties. As a result, generating finer boundaries and summaries that account for these irregularities was difficult.

Lastly, we also test the LLM’s PostGIS generation for ClimateSOM by test generating 20 queries for each of the three categories and manually inspecting the results. We found that our LLM’s generation was accurate in ~90% of the cases, with the remaining ~10% being cases where the LLM generated a query with incorrect syntax. **In all, we found the failure cases with our LLM integration arising mainly from ambiguous region identifiers for spatial tasks, the county-level unit of analysis, and incorrect syntax generation for the PostGIS queries.** A conversational interface that can allow the user to correct the LLM when they generate unreasonable results is a future direction.

7 EXPERT FEEDBACK

In addition to the two experts, **E1** and **E2**, who provided the two case studies, we also solicit feedback on ClimateSOM with a semi-structured interview from four other domain experts, **E3 - E6**, (total of six) by presenting the case studies and the system to them. These experts range in years of experience from 12 to 48 years in climate science and all have worked with climate ensemble datasets. We summarize and discuss the feedback on ClimateSOM below.

On the LLM integration Since the case studies were conducted by experts who had already become familiar with the SOM nodes, thus able to rely on their past knowledge to provide annotations, we instead asked experts to test the potential of LLM integration. The experts found the LLM integration particularly useful in certain circumstances. **E2** and **E3** agreed that LLM integration would be useful if the user had a specific administrative region of their interest. **E1** suggested that the integration would be useful if the geospatial region in question was unfamiliar to them. When visual inspection of the SOM nodes alone is insufficient to understand particular patterns in the SOM Node Space, experts *agreed* that the LLM can be used to both identify regions of interest and to provide textual summaries of the nodes in those regions. However, **E3** questioned the reliability of LLMs in providing sensemaking of the SOM Node Space, suggesting visual inspection of the SOM Node Space may be more reliable. A conversational interface for the LLMs to provide a way to error-correct is a future direction.

On the distributional nature of our data abstraction Throughout the case studies, we saw examples of how the distributional nature of our data abstraction of model runs in ClimateSOM revealed important patterns. Crucially, as **E1** agreed, providing a distributional view of model runs above an interpretable space via the steerable DR, annotations, and LLM-empowered sensemaking, experts can quickly identify and understand crucial characteristics of model runs. **E6** showed significant interest in the descriptive power of our representation, in particular of the vector field formulation of comparison, and noted that they had “*never seen anything like it before.*” Experts agreed that this distributional nature of data abstraction is a **novel way to visualize climate ensemble datasets** and a distinguishing feature of ClimateSOM.

ClimateSOM can quickly discover novel and meaningful insights Most importantly, *all experts* agreed that the insights our system uncovers in climate ensemble datasets are valuable—either because they can be identified or because identifying them manually would require a very substantial effort. **E2** remarked that, to generate similar insights “(their) other methods would involve generating a very large number

of static plots and sifting through them.” **E1** and **E6** also noted the ability to investigate the monthly evolution of the clustering results in ClimateSOM as a novel and valuable feature. **E4** was impressed and suggested that it could also be used to answer other important questions for climate models, such as whether downscaled coarse-resolution global climate models can capture the characteristics of the climate system by comparing it with high-resolution regional climate models. The feedback gives us confidence that our workflow can generate novel insights into climate ensemble datasets of climatological significance.

8 LIMITATIONS AND FUTURE WORK

Despite the overall very positive feedback, experts also pointed out limitations. First, some experts noted the **visual complexity of the workflow and interface**, though they positively reviewed the memorability of the interface (i.e., there is a learning curve to the system, but once learned, it is easy to remember how to use it). Granted, the scope of tasks that ClimateSOM attempts to address is large and complex, and thus future work will focus on improving the usability of the system with better onboarding tutorials. Second, compared to common statistical or analytic methods, ClimateSOM provides **no native metrics of statistical significance** in its findings. Statistical tests are commonly used in climate science to assert anomalous patterns, for example, and the inclusion of such metrics within the ClimateSOM framework is a future direction. Third, although scalability is not a concern for the Model Run Inspection Views, **the scalability of the Clustering View** can become a concern when considering datasets with more model runs. An alternative encoding design to accommodate larger number of model runs is future work. In addition, as introduced in **Sec. 3**, the abstraction in ClimateSOM **ignores the temporal ordering of the model runs** which is of interest to many climate scientists. Finally, in both case studies, SOM training took ~10 minutes. However, **training time will grow linearly with the grid size** potentially making it difficult to find appropriate parameters kR and kS . Furthermore, especially at large grid sizes, Euclidean distance may not be an appropriate metric [28] to compare climate scalar fields, and thus we face this limitation.

9 CONCLUSION

In this paper, we introduce ClimateSOM, a novel visual analysis workflow for climate ensemble datasets. Past works show promise for visual analytics to unravel such complex datasets, but they do not simultaneously address the three key tasks, exploration of a single set of model runs, comparison of two sets of model runs, and clustering of model runs and GCMs, that we identify in collaboration with a domain expert. We leverage self-organizing maps, steerable DR, LLM-empowered query system to address these tasks, and present new insights into a precipitation ensemble dataset over two different regions. We gathered feedback from six domain experts and confirmed that ClimateSOM can uncover climatologically significant insights—many of which are novel or would otherwise require substantial manual effort—provided that the trained SOM *sufficiently* represents the ensemble. We also discuss the limitations of ClimateSOM and suggest future directions, in particular, the integration of statistical tests to quantify the significance of the insights generated by ClimateSOM. We encourage future work in incorporating novel visual analytics techniques to address the unique challenges in climate science.

ACKNOWLEDGMENTS

This research is supported in part by the National Science Foundation via grant No. IIS-2427770

REFERENCES

- [1] Build a Question/Answering system over SQL data. https://python.langchain.com/docs/tutorials/sql_qa/. 12
- [2] LangChain — langchain.com. <https://www.langchain.com>. 5
- [3] J. Achiam, S. Adler, S. Agarwal, L. Ahmad, I. Akkaya, F. L. Aleman, D. Almeida, J. Altenschmidt, S. Altman, S. Anadkat, et al. GPT-4 technical report. *arXiv preprint arXiv:2303.08774*, 2023. doi: 10.48550/arXiv.2303.08774 5
- [4] A. Agrawal, A. Ali, and S. Boyd. Minimum-distortion embedding. *Foundations and Trends in Machine Learning*, 14(3):211–378, 2021. doi: 10.1561/2200000090 4
- [5] G. Andrienko, N. Andrienko, S. Bremm, T. Schreck, T. Von Landesberger, P. Bak, and D. Keim. Space-in-Time and Time-in-Space Self-Organizing Maps for Exploring Spatiotemporal Patterns. *Computer Graphics Forum*, 29(3):913–922, 2010. doi: 10.1111/j.1467-8659.2009.01664.x 2
- [6] K. Bensema, L. Gosink, H. Obermaier, and K. I. Joy. Modality-driven classification and visualization of ensemble variance. *IEEE Transactions on Visualization and Computer Graphics*, 22(10):2289–2299, 2016. doi: 10.1109/TVCG.2015.2507569 1
- [7] J. Bernard, M. Hutter, M. Zeppelzauer, D. Fellner, and M. Sedlmair. Comparing Visual-Interactive Labeling with Active Learning: An Experimental Study. *IEEE Transactions on Visualization and Computer Graphics*, 24(1):298–308, Jan. 2018. doi: 10.1109/TVCG.2017.2744818 2
- [8] A. Biswas, G. Lin, X. Liu, and H.-W. Shen. Visualization of time-varying weather ensembles across multiple resolutions. *IEEE transactions on visualization and computer graphics*, 23(1):841–850, 2016. doi: 10.1109/TVCG.2016.2598869 1
- [9] A. Biswas, G. Lin, X. Liu, and H.-W. Shen. Visualization of Time-Varying Weather Ensembles across Multiple Resolutions. *IEEE Transactions on Visualization and Computer Graphics*, 23(1):841–850, Jan. 2017. doi: 10.1109/TVCG.2016.2598869 1
- [10] R. J. Campello, D. Moulavi, and J. Sander. Density-based clustering based on hierarchical density estimates. In *Pacific-Asia conference on knowledge discovery and data mining*, pp. 160–172. Springer, 2013. doi: 10.1007/978-3-642-37456-2_14 5
- [11] S. Chen, D. Amid, O. M. Shir, L. Limonad, D. Boaz, A. Anaby-Tavor, and T. Schreck. Self-organizing maps for multi-objective pareto frontiers. In *2013 IEEE Pacific Visualization Symposium (PacificVis)*, pp. 153–160, Feb. 2013. doi: 10.1109/PacificVis.2013.6596140 2
- [12] D. Chushig-Muzo, C. Soguero-Ruiz, A. P. Engelbrecht, P. De Miguel Bohoyo, and I. Mora-Jiménez. Data-Driven Visual Characterization of Patient Health-Status Using Electronic Health Records and Self-Organizing Maps. *IEEE Access*, 8:137019–137031, 2020. doi: 10.1109/ACCESS.2020.3012082 2
- [13] B. Efron. Bootstrap methods: another look at the jackknife. In *Breakthroughs in statistics: Methodology and distribution*, pp. 569–593. Springer, 1992. doi: 10.1214/aos/1176344552 5
- [14] J. Eirich, J. Bonart, D. Jäckle, M. Sedlmair, U. Schmid, K. Fischbach, T. Schreck, and J. Bernard. IRVINE: A Design Study on Analyzing Correlation Patterns of Electrical Engines. *IEEE Transactions on Visualization and Computer Graphics*, 28(1):11–21, Jan. 2022. doi: 10.1109/TVCG.2021.3114797 2
- [15] M. Evers, M. Böttinger, and L. Linsen. Interactive Visual Analysis of Regional Time Series Correlation in Multi-field Climate Ensembles. In S. Dutta, K. Feige, K. Rink, and D. Zeckzer, eds., *Workshop on Visualisation in Environmental Sciences (EnvirVis)*. The Eurographics Association, 2023. doi: 10.2312/envirvis.20231108 1
- [16] M. Evers, K. Huesmann, and L. Linsen. Uncertainty-aware Visualization of Regional Time Series Correlation in Spatio-temporal Ensembles. *Computer Graphics Forum*, 40(3):519–530, June 2021. doi: 10.1111/cgf.14326 2
- [17] V. Eyring, S. Bony, G. A. Meehl, C. A. Senior, B. Stevens, R. J. Stouffer, and K. E. Taylor. Overview of the Coupled Model Intercomparison Project Phase 6 (CMIP6) experimental design and organization. *Geoscientific Model Development*, 9(5):1937–1958, 2016. doi: 10.5194/gmd-9-1937-2016 1, 2, 7
- [18] F. Ferstl, M. Kanzler, M. Rautenhaus, and R. Westermann. Time-Hierarchical Clustering and Visualization of Weather Forecast Ensembles. *IEEE Transactions on Visualization and Computer Graphics*, 23(1):831–840, Jan. 2017. doi: 10.1109/TVCG.2016.2598868 1, 2
- [19] R. Flamary, N. Courty, A. Gramfort, M. Z. Alaya, A. Boisbunon, S. Chambon, L. Chapel, A. Corenflos, K. Fatras, N. Fournier, L. Gautheron, N. T. Gayraud, H. Janati, A. Rakotomamonjy, I. Redko, A. Rolet, A. Schutz, V. Seguy, D. J. Sutherland, R. Tavenard, A. Tong, and T. Vayer. POT: Python optimal transport. *Journal of Machine Learning Research*, 22(78):1–8, 2021. 5
- [20] F. Forest, M. Lebbah, H. Azzag, and J. Lacaille. A survey and implementation of performance metrics for self-organized maps. *arXiv preprint arXiv:2011.05847*, 2020. doi: 10.48550/arXiv.2011.05847 14
- [21] P. B. Gibson, S. E. Perkins-Kirkpatrick, P. Uotila, A. S. Pepler, and L. V. Alexander. On the use of self-organizing maps for studying climate extremes. *Journal of Geophysical Research: Atmospheres*, 122(7):3891–3903, 2017. doi: 10.1002/2016JD026256 2, 3, 14
- [22] S. Hemmati, P. Capak, M. Pourrahmani, H. Nayyeri, D. Stern, B. Mobasher, B. Darvish, I. Davidzon, O. Ilbert, D. Masters, and A. Shahidi. Bringing Manifold Learning and Dimensionality Reduction to SED Fitters. *The Astrophysical Journal Letters*, 881(1):L14, Aug. 2019. doi: 10.3847/2041-8213/ab3418 2
- [23] B. C. Hewitson and R. G. Crane. Self-organizing maps: applications to synoptic climatology. *Climate Research*, 22(1):13–26, 2002. doi: 10.3354/cr022013 2
- [24] M. Hutchinson, R. Jianu, A. Slingsby, and P. Madhyastha. LLM-Assisted Visual Analytics: Opportunities and Challenges. In D. Hunter and A. Slingsby, eds., *Computer Graphics and Visual Computing (CGVC)*. The Eurographics Association, 2024. doi: 10.2312/cgvc.20241237 2
- [25] T. Höllt, A. Magdy, P. Zhan, G. Chen, G. Gopalakrishnan, I. Hoteit, C. D. Hansen, and M. Hadwiger. Ovis: A framework for visual analysis of ocean forecast ensembles. *IEEE Transactions on Visualization and Computer Graphics*, 20(8):1114–1126, 2014. doi: 10.1109/TVCG.2014.2307892 1
- [26] T. Ise and Y. Oba. VARENN: graphical representation of periodic data and application to climate studies. *npj Climate and Atmospheric Science*, 3(1):1–6, July 2020. doi: 10.1038/s41612-020-0129-x 2
- [27] D. Jäckle, F. Fischer, T. Schreck, and D. A. Keim. Temporal mds plots for analysis of multivariate data. *IEEE Transactions on Visualization and Computer Graphics*, 22(1):141–150, 2016. doi: 10.1109/TVCG.2015.2467553 7
- [28] C. Kappe. *Visual Analysis of Variability and Features of Climate Simulation Ensembles*. PhD thesis, Dissertation, Kaiserslautern, Technische Universität Kaiserslautern, 2022, 2022. 2, 9
- [29] C. Kappe, M. Böttinger, and H. Leitte. Analysis of Decadal Climate Predictions with User-guided Hierarchical Ensemble Clustering. *Computer Graphics Forum*, 38(3):505–515, 2019. doi: 10.1111/cgf.13706 2
- [30] C. Kappe, M. Böttinger, and H. Leitte. Topology-based feature analysis of scalar field ensembles: An application to climate (change) analysis. *Computers & Graphics*, 104:59–71, 2022. doi: 10.1016/j.cag.2022.03.004 1
- [31] C. P. Kappe, M. Böttinger, and H. Leitte. Exploring Variability within Ensembles of Decadal Climate Predictions. *IEEE Transactions on Visualization and Computer Graphics*, 25(3):1499–1512, Mar. 2019. doi: 10.1109/TVCG.2018.2810919 1, 2
- [32] C. P. Kappe, M. Böttinger, and H. Leitte. Topology-based Feature Detection in Climate Data. In R. Bujack, K. Feige, K. Rink, and D. Zeckzer, eds., *Workshop on Visualisation in Environmental Sciences (EnvirVis)*. The Eurographics Association, 2019. doi: 10.2312/envirvis.20191099 1
- [33] J. Kehrer, P. Filzmoser, and H. Hauser. Brushing Moments in Interactive Visual Analysis. *Computer Graphics Forum*, 29(3):813–822, June 2010. doi: 10.1111/j.1467-8659.2009.01697.x 1
- [34] J. Kehrer and H. Hauser. Visualization and visual analysis of multifaceted scientific data: A survey. *IEEE Transactions on Visualization and Computer Graphics*, 19(3):495–513, 2013. doi: 10.1109/TVCG.2012.110 1
- [35] T. Kohonen. The self-organizing map. *Proceedings of the IEEE*, 78(9):1464–1480, Sept. 1990. doi: 10.1109/5.58325 1, 2
- [36] B. Li, Y. Luo, C. Chai, G. Li, and N. Tang. The Dawn of Natural Language to SQL: Are We Fully Ready? *Proceedings of the VLDB Endowment*, 17(11):3318–3331, July 2024. doi: 10.14778/3681954.3682003 2
- [37] H. Li, W. Kam-Kwai, Y. Luo, J. Chen, C. Liu, Y. Zhang, A. K. H. Lau, H. Qu, and D. Liu. Save It for the "Hot" Day: An LLM-Empowered Visual Analytics System for Heat Risk Management, June 2024. arXiv:2406.03317 [cs]. doi: 10.48550/arXiv.2406.03317 2
- [38] L. Liu, M. Mirzargar, R. Kirby, R. Whitaker, and D. H. House. Visualizing Time-Specific Hurricane Predictions, with Uncertainty, from Storm Path Ensembles. *Computer Graphics Forum*, 34(3):371–380, 2015. doi: 10.

- [39] M. Liu, X. Wang, J. Xu, H. Lu, and Y. Tong. NALSpatial: A Natural Language Interface for Spatial Databases. *IEEE Transactions on Knowledge and Data Engineering*, pp. 1–14, 2025. doi: [10.1109/TKDE.2025.3525587](https://doi.org/10.1109/TKDE.2025.3525587) 4
- [40] M. X. Liu, T. Wu, T. Chen, F. M. Li, A. Kittur, and B. A. Myers. Selenite: Scaffolding Online Sensemaking with Comprehensive Overviews Elicited from Large Language Models. In *Proceedings of the CHI Conference on Human Factors in Computing Systems*, pp. 1–26. ACM, Honolulu HI USA, May 2024. doi: [10.1145/3613904.3642149](https://doi.org/10.1145/3613904.3642149) 2
- [41] Y. Liu, R. H. Weisberg, Y. Liu, and R. H. Weisberg. A Review of Self-Organizing Map Applications in Meteorology and Oceanography. In *Self Organizing Maps - Applications and Novel Algorithm Design*. IntechOpen, Jan. 2011. doi: [10.5772/13146](https://doi.org/10.5772/13146) 2
- [42] Y. Liu, R. H. Weisberg, and C. N. K. Mooers. Performance evaluation of the self-organizing map for feature extraction. *Journal of Geophysical Research: Oceans*, 111(C5), 2006. doi: [10.1029/2005JC003117](https://doi.org/10.1029/2005JC003117) 2
- [43] B. Ma and A. Entezari. An Interactive Framework for Visualization of Weather Forecast Ensembles. *IEEE Transactions on Visualization and Computer Graphics*, 25(1):1091–1101, Jan. 2019. doi: [10.1109/TVCG.2018.2864815](https://doi.org/10.1109/TVCG.2018.2864815) 1
- [44] N. Maher, S. Milinski, L. Suarez-Gutierrez, M. Botzet, M. Dobrynin, L. Kornbluh, J. Kröger, Y. Takano, R. Ghosh, C. Hedemann, C. Li, H. Li, E. Manzini, D. Notz, D. Putrasahan, L. Boysen, M. Claussen, T. Ilyina, D. Olonschek, T. Raddatz, B. Stevens, and J. Marotzke. The Max Planck Institute Grand Ensemble: Enabling the Exploration of Climate System Variability. *Journal of Advances in Modeling Earth Systems*, 11(7):2050–2069, 2019. doi: [10.1029/2019MS001639](https://doi.org/10.1029/2019MS001639) 1
- [45] L. McInnes, J. Healy, and J. Melville. Umap: Uniform manifold approximation and projection for dimension reduction. *arXiv preprint arXiv:1802.03426*, 2018. doi: [10.48550/arXiv.1802.03426](https://doi.org/10.48550/arXiv.1802.03426) 4
- [46] H. Mihanović, S. Cosoli, I. Vilibić, D. Ivanković, V. Dadić, and M. Gačić. Surface current patterns in the northern Adriatic extracted from high-frequency radar data using self-organizing map analysis. *Journal of Geophysical Research: Oceans*, 116(C8), 2011. doi: [10.1029/2011JC007104](https://doi.org/10.1029/2011JC007104) 2
- [47] J. M. Murphy, D. M. H. Sexton, D. N. Barnett, G. S. Jones, M. J. Webb, M. Collins, and D. A. Stainforth. Quantification of modelling uncertainties in a large ensemble of climate change simulations. *Nature*, 430(7001):768–772, Aug. 2004. doi: [10.1038/nature02771](https://doi.org/10.1038/nature02771) 1
- [48] J. M. Patchett and G. R. Gislser. Deep water impact ensemble data set. Technical Report LA-UR-17-21595, Los Alamos National Laboratory, May 2017. 1
- [49] D. W. Pierce, D. R. Cayan, D. R. Feldman, and M. D. Risser. Future increases in North American extreme precipitation in CMIP6 downscaled with LOCA. *Journal of Hydrometeorology*, 24(5):951–975, 2023. doi: [10.1175/JHM-D-22-0194.1](https://doi.org/10.1175/JHM-D-22-0194.1) 1, 7
- [50] D. W. Pierce, D. R. Cayan, E. P. Maurer, J. T. Abatzoglou, and K. C. Hegewisch. Improved bias correction techniques for hydrological simulations of climate change. *Journal of Hydrometeorology*, 16(6):2421–2442, 2015. doi: [10.1175/JHM-D-14-0236.1](https://doi.org/10.1175/JHM-D-14-0236.1) 7
- [51] D. W. Pierce, D. R. Cayan, and B. L. Thrasher. Statistical downscaling using localized constructed analogs (LOCA). *Journal of hydrometeorology*, 15(6):2558–2585, 2014. doi: [10.1175/JHM-D-14-0082.1](https://doi.org/10.1175/JHM-D-14-0082.1) 7
- [52] X. Pu, M. Gao, and X. Wan. Summarization is (Almost) Dead. *arXiv preprint arXiv:2309.09558*, Sept. 2023. doi: [10.48550/arXiv.2309.09558](https://doi.org/10.48550/arXiv.2309.09558) 4
- [53] K. Quintelier, A. Couckuyt, A. Emmaneel, J. Aerts, Y. Saeys, and S. Van Gassen. Analyzing high-dimensional cytometry data using FlowSOM. *Nature Protocols*, 16(8):3775–3801, Aug. 2021. doi: [10.1038/s41596-021-00550-0](https://doi.org/10.1038/s41596-021-00550-0) 2
- [54] M. D. Rahman, G. J. Quadri, B. Doppalapudi, D. A. Szafir, and P. Rosen. A Qualitative Analysis of Common Practices in Annotations: A Taxonomy and Design Space. *IEEE Transactions on Visualization and Computer Graphics*, 31(1):360–370, Jan. 2025. Conference Name: IEEE Transactions on Visualization and Computer Graphics. doi: [10.1109/TVCG.2024.3456359](https://doi.org/10.1109/TVCG.2024.3456359) 2
- [55] D. B. Reusch, R. B. Alley, and B. C. Hewitson. North Atlantic climate variability from a self-organizing map perspective. *Journal of Geophysical Research: Atmospheres*, 112(D2), 2007. doi: [10.1029/2006JD007460](https://doi.org/10.1029/2006JD007460) 2
- [56] K. Riahi, D. P. Van Vuuren, E. Kriegler, J. Edmonds, B. C. O’neill, S. Fujimori, N. Bauer, K. Calvin, R. Dellink, O. Fricko, et al. The shared socioeconomic pathways and their energy, land use, and greenhouse gas emissions implications: An overview. *Global environmental change*, 42:153–168, 2017. doi: [10.1016/j.gloenvcha.2016.05.009](https://doi.org/10.1016/j.gloenvcha.2016.05.009) 2, 7
- [57] D. Sacha, M. Kraus, J. Bernard, M. Behrisch, T. Schreck, Y. Asano, and D. A. Keim. SOMFlow: Guided Exploratory Cluster Analysis with Self-Organizing Maps and Analytic Provenance. *IEEE Transactions on Visualization and Computer Graphics*, 24(1):120–130, Jan. 2018. doi: [10.1109/TVCG.2017.2744805](https://doi.org/10.1109/TVCG.2017.2744805) 2
- [58] J. Sammon. A nonlinear mapping for data structure analysis. *IEEE Transactions on Computers*, C-18(5):401–409, 1969. doi: [10.1109/T-C.1969.222678](https://doi.org/10.1109/T-C.1969.222678) 3
- [59] J. Sanyal, S. Zhang, J. Dyer, A. Mercer, P. Amburn, and R. Moorhead. Noodles: A Tool for Visualization of Numerical Weather Model Ensemble Uncertainty. *IEEE Transactions on Visualization and Computer Graphics*, 16(6):1421–1430, Nov. 2010. doi: [10.1109/TVCG.2010.181](https://doi.org/10.1109/TVCG.2010.181) 1
- [60] L. Shen, E. Shen, Y. Luo, X. Yang, X. Hu, X. Zhang, Z. Tai, and J. Wang. Towards Natural Language Interfaces for Data Visualization: A Survey. *IEEE Transactions on Visualization and Computer Graphics*, 29(6):3121–3144, June 2023. doi: [10.1109/TVCG.2022.3148007](https://doi.org/10.1109/TVCG.2022.3148007) 2
- [61] S. C. Sheridan and C. C. Lee. The self-organizing map in synoptic climatological research. *Progress in Physical Geography: Earth and Environment*, 35(1):109–119, Feb. 2011. doi: [10.1177/0309133310397582](https://doi.org/10.1177/0309133310397582) 2, 3
- [62] Q. Shu, H. Guo, J. Liang, L. Che, J. Liu, and X. Yuan. Ensemblegraph: Interactive visual analysis of spatiotemporal behaviors in ensemble simulation data. In *2016 IEEE Pacific Visualization Symposium (PacificVis)*, pp. 56–63. IEEE, 2016. doi: [10.1109/PACIFICVIS.2016.7465251](https://doi.org/10.1109/PACIFICVIS.2016.7465251) 2
- [63] Y. Tu, R. Qiu, Y.-S. Wang, P.-Y. Yen, and H.-W. Shen. PhraseMap: Attention-Based Keyphrases Recommendation for Information Seeking. *IEEE Transactions on Visualization and Computer Graphics*, 30(3):1787–1802, Mar. 2024. doi: [10.1109/TVCG.2022.3225114](https://doi.org/10.1109/TVCG.2022.3225114) 2
- [64] S. Van Gassen, B. Callebaut, M. J. Van Helden, B. N. Lambrecht, P. De-meester, T. Dhaene, and Y. Saeys. FlowSOM: Using self-organizing maps for visualization and interpretation of cytometry data. *Cytometry. Part A: The Journal of the International Society for Analytical Cytology*, 87(7):636–645, July 2015. doi: [10.1002/cyto.a.22625](https://doi.org/10.1002/cyto.a.22625) 2
- [65] V. M. Vu, A. Bibal, and B. Frénay. Integrating Constraints Into Dimensionality Reduction for Visualization: A Survey. *IEEE Transactions on Artificial Intelligence*, 3(6):944–962, Dec. 2022. doi: [10.1109/TAI.2022.3204734](https://doi.org/10.1109/TAI.2022.3204734) 4
- [66] J. Wang, S. Hazarika, C. Li, and H.-W. Shen. Visualization and Visual Analysis of Ensemble Data: A Survey. *IEEE Transactions on Visualization and Computer Graphics*, 25(9):2853–2872, Sept. 2019. doi: [10.1109/TVCG.2018.2853721](https://doi.org/10.1109/TVCG.2018.2853721) 1
- [67] J. Wang, X. Liu, H.-W. Shen, and G. Lin. Multi-Resolution Climate Ensemble Parameter Analysis with Nested Parallel Coordinates Plots. *IEEE Transactions on Visualization and Computer Graphics*, 23(1):81–90, Jan. 2017. doi: [10.1109/TVCG.2016.2598830](https://doi.org/10.1109/TVCG.2016.2598830) 1
- [68] Y. Wu, L. Yan, L. Shen, Y. Wang, N. Tang, and Y. Luo. ChartInsights: Evaluating Multimodal Large Language Models for Low-Level Chart Question Answering, Nov. 2024. arXiv:2405.07001 [cs]. doi: [10.48550/arXiv.2405.07001](https://doi.org/10.48550/arXiv.2405.07001) 2
- [69] W. Zhang, Y. Wang, Y. Song, V. J. Wei, Y. Tian, Y. Qi, J. H. Chan, R. C.-W. Wong, and H. Yang. Natural Language Interfaces for Tabular Data Querying and Visualization: A Survey. *IEEE Transactions on Knowledge and Data Engineering*, 36(11):6699–6718, Nov. 2024. doi: [10.1109/TKDE.2024.3400824](https://doi.org/10.1109/TKDE.2024.3400824) 2, 4
- [70] Y. Zhao, Y. Zhang, Y. Zhang, X. Zhao, J. Wang, Z. Shao, C. Turkay, and S. Chen. LEVA: Using Large Language Models to Enhance Visual Analytics. *IEEE Transactions on Visualization and Computer Graphics*, 31(3):1830–1847, Mar. 2025. Conference Name: IEEE Transactions on Visualization and Computer Graphics. doi: [10.1109/TVCG.2024.3368060](https://doi.org/10.1109/TVCG.2024.3368060) 2

A PROMPTS USED IN THE LLM INTEGRATION

A.1 Forward Direction

In the forward direction, we presume the user has a SOM node characteristic in mind, (e.g. “*Show me SOM nodes with average above 0 over Southern California*”) and we wish to identify a region within the Adjusted SOM Node Space that corresponds to this requested characteristic. To this end, we want to build an appropriate PostGIS query that matches the user’s request. Using LangChain, we first detect any spatial region (e.g. *Southern California*) using LangChain Tools. If so, we first use the Region to Counties prompt to identify the counties in the region. Once we have the counties, for which strict definitions are available, we obtain the boundaries for the region in the original query. Next the PostGIS Prompt Generation prompt, along with the LangChain Tool Calling that automatically supplies the computed boundary, is used to generate the PostGIS query. We note that the SQL query generation prompt is loosely based on LangChain’s documentation on SQL generation [1]. Finally, we use the Clean Query prompt to ensure the query is syntactically correct and complete.

PROMPT: Region to Counties

Given a US region in the West coast, return the names and states of the counties in that region.
Region: {{ Region }}

PROMPT: PostGIS Prompt Generation

Pay attention to use only the column names that you can see in the schema description. Be careful to not query for columns that do not exist. Do not use the lat or lon columns. Always build valid and complete SRID 4326 PostGIS polygons for the region specified in the question.

Example:

Question: grid_ids whose average value in the Southern California higher than 0.5

Answer:

```
SELECT grid_id FROM spatial_data WHERE ST_Intersects(geom, ST_GeomFromText(<polygon text>, 4326)) GROUP BY grid_id HAVING AVG(value) > 0.5;
```

Question: grid_ids with average higher within Central Valley in California than Southern California

Answer:

```
WITH polygon_a_values AS (
SELECT
  grid_id,
  AVG(value) as avg_value_a
FROM your_table
WHERE ST_Contains(ST_GeomFromText(<polygon text>, 4326), geom)

GROUP BY grid_id
),
polygon_b_values AS (
SELECT
  grid_id,
  AVG(value) as avg_value_b
FROM your_table
WHERE ST_Contains(ST_GeomFromText(<polygon text>, 4326), geom)
GROUP BY grid_id
)
SELECT a.grid_id
FROM polygon_a_values a
JOIN polygon_b_values b
ON a.grid_id = b.grid_id
WHERE a.avg_value_a > b.avg_value_b;
```

Only use the following table: {{table_schema}}

Question: {{question}}

Write an initial draft of the query. Then double check the PostGIS query for common mistake. Produce just the queries. Don’t comment on the changes.

Changes may include:

- ST_ functions are used with the right parameters
- Specify SRID 4326 for all geometries
- Using NOT IN with NULL values
- Using UNION when UNION ALL should have been used
- Using BETWEEN for exclusive ranges
- Data type mismatch in predicates
- Properly quoting identifiers
- Using the correct number of arguments for functions
- Casting to the correct data type
- Using the proper columns for joins

Use format:

First draft: <<FIRST_DRAFT_QUERY>>

Final answer: <<FINAL_ANSWER_QUERY>>

PROMPT: Clean Query

Clean the following into an one-line query with no extra text and make sure its a valid PostGIS query and specify SRID 4326: {{to_be_cleaned}}

A.1.1 Example

1. **User Query:** grid_ids whose average value over Southern California is higher than 0.
2. Detect *Southern California* as a region that needs to be resolved.
3. Resolve *Southern California* to the following counties:

Los Angeles County-CA, San Diego County-CA, Orange County-CA, Riverside County-CA, San Bernardino County-CA, Ventura County-CA

4. Generate the boundary for *Southern California* by combining the known boundaries for the counties.

```
MULTIPOLYGON ((-118.881656 34.791231, ...))
```

5. Construct the PostGIS query.

Output:

```
SELECT grid_id FROM spatial_data WHERE ST_Intersects(geom, ST_GeomFromText('MULTIPOLYGON (((-118.881656 34.791231, -117.632011 34.82227, -117.632996 35.797251, -115.648357 35.809211, -114.633487 35.001857, -114.386699 34.457911, -114.131211 34.26273, -114.52868 33.947817, -114.627125 33.433554, -116.085165 33.425932, -116.106168 32.61848, -117.204917 32.528832, -117.571531 33.312302, -118.1259 33.697151, -118.466962 33.725524, -118.557356 33.987673, -119.158963 34.040253, -119.500953 34.326922, -119.442352 34.901274, -118.881656 34.791231))), ((-118.659924 33.50576, -118.359393 33.464922, -118.251379 33.353397, -118.241051 33.313029, -118.250903 33.280465, -118.50368 33.285314, -118.659924 33.50576)), ((-118.654363 33.074952, -118.523727 33.059972, -118.298469 32.794257, -118.538197 32.81277, -118.654363 33.074952)), ((-119.634795 33.285956, -119.519138 33.3337, -119.360702 33.221452, -119.512001 33.167755, -119.634795 33.285956)), ((-119.468064 34.063139, -119.330926 34.065064, -119.296238 33.99724, -119.454479
```


Southern California and Central Coast, including the Bay Area.



Fig. 11: Users were asked to rate in a 5-point likert scale how reasonable the LLM-generated summary of drawn boundary was. Question: “How reasonable is the above LLM-generated summary in the map title for the drawn boundary?”

D DETAILS OF THE SOM TRAINING FOR ClimateSOM

D.1 On the metrics for SOM training

Past research have employed various metrics to evaluate the quality of a SOM [20]. Generally, metrics for SOM are divided into those that evaluate error that the SOM approximation introduces and those that evaluate the topological properties of the SOM grid. ClimateSOM requires both classes of metrics to measure that the trained SOM abstraction retains *sufficient* information whilst also ensuring that the MDE dimensionality-reduced space is connected and interpretable. The most common metrics for the respective categories are quantization error (QE) and topographic error (TE). While these are useful metrics, we present two more metrics that we have found useful for ClimateSOM: (1) Explained Variance (EV) and (2) Mean Smoothness (μ_S).

Explained Variance, akin to its definition in principal components analysis (PCA), measures the proportion of variance in the input data set that is explained by the SOM grid, where 0 indicates no explanatory power and 1 indicates full explanatory power. We replace QE with Explained Variance to provide a unitless measure of the explanatory power of the SOM grid.

Mean Smoothness is another metric that we introduce to more carefully evaluate the smoothness of the SOM grid as non smoothness can produce disconnected MDE results. Given a SOM grid G , we define local smoothness, LS , at any grid node $g_{i,j}$ as the average Euclidean distance between $g_{i,j}$ and its four immediate neighbors and define the Mean Smoothness as $\mu_{g_{i,j}}$. We found that topographic error was not sufficient to capture the required smoothness of the SOM grid to ensure the interpretability of the MDE result and thus replace the topology-based error metric with Mean Smoothness.

In all, SOM training for ClimateSOM is the balancing of its explanatory power (QE, EV) and smoothness (μ_S). The following, Appendix D.2, discusses the choice of parameters in the context of these metrics and the implications.

D.2 On the parameter choices for SOM training

Among the parameters required for SOM training the initial neighborhood size (kR) and the neighborhood size decay (kS) are most important and we thus list their influences here.

kR The Gaussian neighborhood function depends on the parameter σ . The term kR defines its initial value as the ratio between the SOM grid area and the neighborhood update area, given by $kR = (\sigma_{initial})^2 / dim^2$. Generally, a larger kR results in a smoother SOM grid with less explanatory power and a smaller kR results in the opposite.

kS In order for the SOM to *fit* the data, it is common to linearly decay the neighborhood size over time [21]. kS defines the final value of the neighborhood size as a ratio of the initial value, $kS = \sigma_{final} / \sigma_{initial}$. Similar to kR , kS also expresses a trade-off between smoothness and explanatory power. A larger kS results in a smoother SOM grid with less explanatory power and a smaller kS results in the opposite.

Other parameters such as the dimensions of the SOM grid, as long as they were sufficiently large to enable sufficient explained variance, learning rate decay, the number of iterations, and the initialization method are part of the training process but were found less critical to the performance, and hence we omit them from discussion. Fig. 12 shows the tradeoff between kR and kS as it relates to the explained variance and mean smoothness – choosing the right parameter is a balance act between the two.

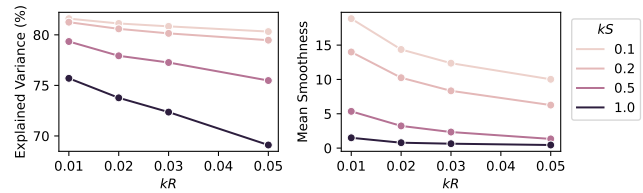


Fig. 12: Effects of SOM Parameters, kR and kS on the explanatory power and smoothness of the SOM grid trained for the California Use Case

E DETAILS OF THE ENSEMBLE MEMBERS USED IN THIS WORK

Global Climate Model (GCM)	Shared Socioeconomic Pathway (SSP)	Variant
ACCESS-CM2	historical	r1i1p1f1
CESM2-LENS	historical	r1i1p1f1
CNRM-ESM2-1	historical	r1i1p1f2
EC-Earth3-Veg	historical	r1i1p1f1
EC-Earth3	historical	r1i1p1f1
FGOALS-g3	historical	r1i1p1f1
GFDL-ESM4	historical	r1i1p1f1
HadGEM3-GC31-LL	historical	r1i1p1f3
INM-CM5-0	historical	r1i1p1f1
IPSL-CM6A-LR	historical	r1i1p1f1
KACE-1-0-G	historical	r1i1p1f1
MIROC6	historical	r1i1p1f1
MPI-ESM1-2-HR	historical	r1i1p1f1
MRI-ESM2-0	historical	r1i1p1f1
TaiESM1	historical	r1i1p1f1
ACCESS-CM2	ssp245	r1i1p1f1
CESM2-LENS	ssp245	r1i1p1f1
EC-Earth3-Veg	ssp245	r1i1p1f1
EC-Earth3	ssp245	r1i1p1f1
FGOALS-g3	ssp245	r1i1p1f1
GFDL-ESM4	ssp245	r1i1p1f1
HadGEM3-GC31-LL	ssp245	r1i1p1f3
INM-CM5-0	ssp245	r1i1p1f1
IPSL-CM6A-LR	ssp245	r1i1p1f1
KACE-1-0-G	ssp245	r1i1p1f1
MIROC6	ssp245	r1i1p1f1
MPI-ESM1-2-HR	ssp245	r1i1p1f1
MRI-ESM2-0	ssp245	r1i1p1f1
TaiESM1	ssp245	r1i1p1f1
ACCESS-CM2	ssp370	r1i1p1f1
CESM2-LENS	ssp370	r1i1p1f1
CNRM-ESM2-1	ssp370	r1i1p1f2
EC-Earth3-Veg	ssp370	r1i1p1f1
EC-Earth3	ssp370	r1i1p1f1
FGOALS-g3	ssp370	r1i1p1f1
GFDL-ESM4	ssp370	r1i1p1f1
INM-CM5-0	ssp370	r1i1p1f1
IPSL-CM6A-LR	ssp370	r1i1p1f1
KACE-1-0-G	ssp370	r1i1p1f1
MIROC6	ssp370	r1i1p1f1
MPI-ESM1-2-HR	ssp370	r1i1p1f1
MRI-ESM2-0	ssp370	r1i1p1f1
TaiESM1	ssp370	r1i1p1f1
ACCESS-CM2	ssp585	r1i1p1f1
CESM2-LENS	ssp585	r1i1p1f1
EC-Earth3-Veg	ssp585	r1i1p1f1
EC-Earth3	ssp585	r1i1p1f1
FGOALS-g3	ssp585	r1i1p1f1
GFDL-ESM4	ssp585	r1i1p1f1
HadGEM3-GC31-LL	ssp585	r1i1p1f3
INM-CM5-0	ssp585	r1i1p1f1
IPSL-CM6A-LR	ssp585	r1i1p1f1
KACE-1-0-G	ssp585	r1i1p1f1
MIROC6	ssp585	r1i1p1f1
MPI-ESM1-2-HR	ssp585	r1i1p1f1
MRI-ESM2-0	ssp585	r1i1p1f1

Table 1: LOCA-Downscaled CMIP6 Precipitation Ensemble members used in this work